Proc. Indian Acad. Sci. (Chem. Sci.), Vol. 93, No. 3, April 1984, pp. 335–355.

Adsorption of carbon monoxide and oxygen on transition metal surfaces: A comparative study of the results from electron spectroscopy and theoretical calculations†

P VISHNU KAMATH, D D SARMA and C N R RAO*

Solid State and Structural Chemistry Unit, Indian Institute of Science, Bangalore 560012, India.

Abstract. Results of investigations on the adsorption of CO and O_2 on transition metal surfaces by employing UV and x-ray photoelectron spectroscopy and electron energy loss spectroscopy (EELS) are presented. Results of molecular orbital calculations on adsorbed CO and O_2 are also discussed. Some of the interesting aspects discussed are, satellites in the O(1*s*) region due to adsorbed CO, vibrational EELS of adsorbed O_2 and dissociation energy profiles of adsorbed O_2 on clean surfaces as well as surfaces covered with potassium or presorbed atomic oxygen.

Keywords. X-ray photoelectron spectroscopy; electron energy loss spectroscopy; carbon monoxide adsorption; oxygen adsorption; transition metal surfaces; dissociation energy profiles.

1. Introduction

Study of the adsorption of gases on metal surfaces has gained renewed importance in the last decade due to the advent of sophisticated surface-sensitive techniques. Carbon monoxide is one of the molecules which has been examined most extensively by photoelectron spectroscopy, electron energy loss spectroscopy and related techniques (Rao and Hegde 1981). Adsorption of CO on transition metals can be molecular or dissociative; furthermore, CO gets adsorbed with several possible geometries. Oxygen is generally adsorbed dissociatively on metals, but molecularly on some metals at low temperatures. Electron spectroscopic techniques have been employed to characterise the adsorbed oxygen species (Rao *et al* 1982; Spitzer and Luth 1982; Kamath and Rao 1984). In this article, we attempt to briefly present the important findings from electron spectroscopic studies of CO and O_2 adsorbed on transition metals and then examine the adsorption of these gases on metal clusters by molecular orbital calculations.

2. Methods of study

2.1 *Experimental*

We have carried out experimental investigations of O_2 and CO adsorbed on transition metal surfaces by employing UPS, XPS and EELS. For this purpose we have used the VG ESCA III mark 2 as well as the VG ESCALAB-EELS spectrometers. The metals were in the form

† Contribution No 245 from the Solid State and Structural Chemistry Unit.

* To whom all correspondence should be addressed.

of polycrystalline foils. The foils were cleaned by repeated heating and etching with Ar ions (Rao *et al* 1980). The XP spectra were continuously monitored to ensure sample cleanliness. The experiments were carried out at low temperature, using a special probe designed for the purpose.

CO and O_2 were purified by repeated distillation in a series of liq N_2 traps and were passed through drying towers. The moisture-free gases were stored in a special gas handling manifold. Exposures were made by leaking the gas into the chamber through a precision leak-valve. Exposures have been measured in Langmuirs ($1\,L = 10^{-6}$ torr sec).

2.2 *Theoretical studies*

We have also investigated the adsorption of O_2 and CO on transition metal surfaces by carrying out extended Hückel calculations (Hoffmann 1963), using standard parameters (Clementi and Raimondi 1963; Baetzold 1971; Zerner and Goutermann 1966). The choice of a suitable metal cluster is crucial for a theoretical study of the adsorption problem. The concept of the use of a cluster in the treatment of the adsorption problem is based on the premise that adsorption is a localized phenomenon. The cluster must be large enough to simulate the properties of an infinite solid, while at the same time it must be within the reach of quantum chemical calculations.

2.3 *Metal clusters*

We have carried out calculations on a series of metal clusters of Cu and Ag: a single metal atom M; a central metal atom (which is the adsorption site) with four nearest neighbours in the same plane, M_5; a M_5 cluster together with the four nearest neighbours in the plane below, M_9. The clusters are constructed in this manner symmetrically around the central atom to produce an FCC structure (figure 1). The orientation selected is the [100] plane. The various cluster properties so calculated are shown in figure 2.

The cohesive energy of a cluster is defined as, $E_{coh} = (nE_{atom} - E_{cluster})/n$ where n is the number of atoms in the cluster. The cohesive energy is plotted in figure 2a as a function of cluster size. We find rough convergence of the cohesive energy for both Cu and Ag. On increasing the cluster size to M_9 from M_5, the cohesive energy changes by only 6%.

The d band width of the clusters is plotted against the cluster size in figure 2b and the energy level diagram of the clusters is given in figure 2c, in order to show how the $(s-p)$ bands and the d band vary with cluster size. From figure 2b, we observe that the d band width passes through a maximum and in the M_9 cluster the d band width is

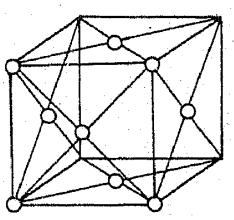

Figure 1. Geometry of the M_9 cluster constructed in the 100 direction of a FCC lattice.

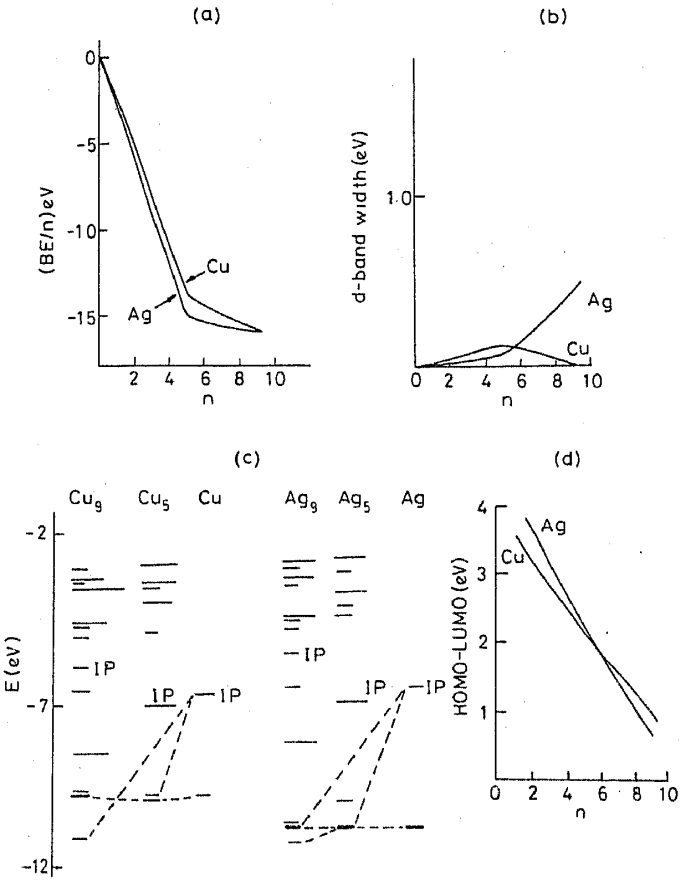

Figure 2. (**a**) Plot of the binding energy per atom as a function of the cluster size, n. (**b**) Plot of the d-band width, $\Delta E_{d\,\text{band}}$, as a function of cluster size, n. (**c**) Energy level diagram of Cu_n and Ag_n clusters where $n = 1$, 5 and 9. The length of the line drawn for each orbital is proportional to the degeneracy. The darker lines represent the spread of the d band. IE stands for the ionization energy. (**d**) Plot of the $\Delta E_{\text{HOMO-LUMO}}$, band gap as a function of cluster size n.

negligible. This is emphasized in the energy level diagram, where the cluster orbitals arising from the atomic d orbitals group together while the $s-p$ derived orbitals spread into a broad band. The bottom of the s band stabilizes greatly as the cluster size increases. In the Cu_5 cluster, the bottom of the s band energetically approaches the d band. In these clusters, substantial mixing of the $4s$ and $3d$ orbitals occurs leading to a greater breadth of the d band (as evidenced by the maximum in figure 2b). In the M_9 clusters, however, the bottom of the s band stabilizes far below the d band. In the case of Ag, the s band does not stabilize below the d band even in the nine-atom cluster.

The energy difference between the HOMO and the LUMO orbitals decreases with increase in the cluster size (figure 2d) as we would expect in the case of metals.

In these finite clusters, there is charge transfer from one set of symmetrically equivalent atoms to another set of symmetrically equivalent atoms (average charges are shown in table 1). The central atom receives electrons in the Cu_5 cluster, while in the Cu_9 cluster, the whole of the upper plane of five atoms acts as an electron donor and assumes a positive charge. The charge on the atoms in the Cu_9 cluster is much lower

Table 1. Average charge on the metal atoms within the Cu clusters.

Cu		Cu_5		Cu_9	
Atom	Charge	Atom	Charge	Atom	Charge
1	0·0	1	−0·356	1	0·026
—	—	2, 3, 4, 5	0·089	2, 3, 4, 5	0·042
—	—	—	—	6, 7, 8, 9	−0·049

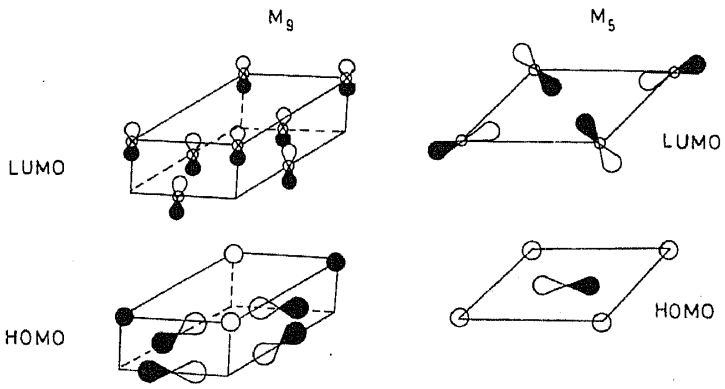

Figure 3. Frontier orbitals of Cu_5 and Cu_9 clusters.

compared to the Cu_5 cluster, indicating the effect of the cluster size. With smaller charges, the Cu_9 cluster is adequately close to the real metal situation.

The *d* orbitals contribute little to bonding within the cluster and remain more or less close to their atomic energy positions. The 4*s* and 4*p* orbitals are greatly perturbed from their atomic energies and give rise to bonding within the cluster through overlap of both σ and π orbitals. The HOMO and LUMO orbitals of the nine atom and five atom Cu clusters are shown in figure 3. The HOMO as well as the LUMO of the five-atom cluster are of the σ kind with the HOMO having a contribution from the central Cu atom. In the Cu_9 cluster, the HOMO has no contribution from the central Cu atom and is of the σ kind; the LUMO on the other hand, is a π type of orbital. The LUMO has predominent contribution from the p_z atomic orbitals and is symmetrically suited to interact with the adsorbate orbitals.

In order to investigate the effect of the cluster size on adsorption, we have performed calculations on the adsorption of oxygen on different clusters in the linear on-top geometry. Potential energy curves for the interaction of oxygen with M, M_5 and M_9 copper clusters are shown in figure 4. The potential energy curve is both steep and deep for the CuO_2 cluster, predicting good metal-oxygen bonding. Inclusion of the first nearest neighbours in the same plane tends to reduce this metal-adsorbate bonding, resulting in a shallow potential energy curve for the Cu_5O_2 cluster. This is indicative of strong intracluster bonding, which reduces the strength of the extra cluster bonds. Furthermore, the frontier orbitals of the Cu_5 cluster are of the in-plane σ kind and are not suited for interaction with the adsorbate orbitals. The absence of strong metal-adsorbate bonding is therefore an artefact of cluster size. Inclusion of the atoms of the

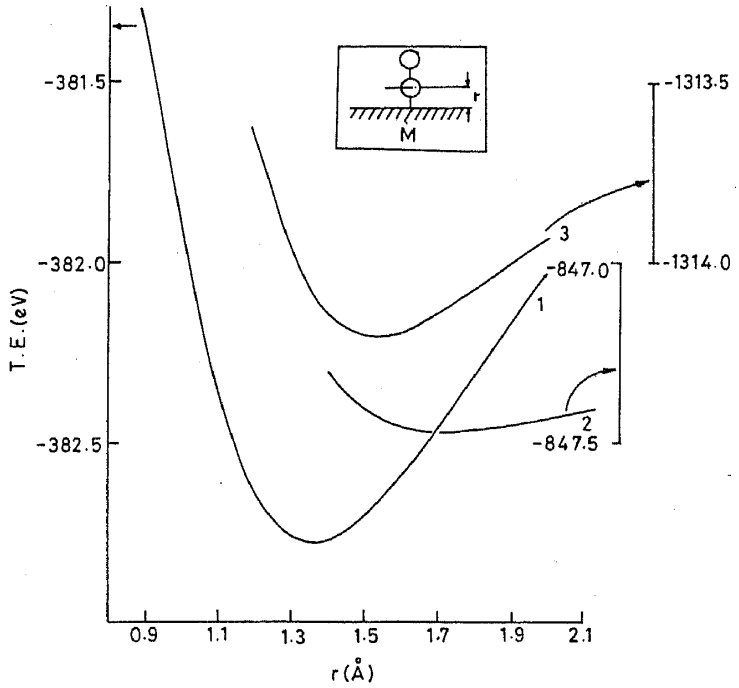

Figure 4. Potential energy curves for the interaction of an oxygen molecule with $(M)_n$ clusters: curve 1, $n = 1$; curve 2, $n = 5$; curve 3, $n = 9$. The Y axis for each curve is drawn separately. Inset shows the geometry of the calculation.

plane below, as in the Cu_9 cluster, improves the situation and adequate bonding for the Cu_9O_2 cluster can be predicted.

The calculated values of the equilibrium metal-oxygen distance do not follow any pattern as a function of cluster size, the distances being, $d(M-O_2) = 1{\cdot}4$ Å, $d(M_5-O_2) = 1{\cdot}7$ Å and $d(M_9-O_2) = 1{\cdot}5$ Å.

It appears that a M_5 cluster is an inadequate representation of the bulk metal and a larger cluster of the size of M_9 is necessary for the cluster treatment of adsorption in the EHT framework.

3. Experimental results on the adsorption of CO on transition metals

Adsorption of CO has been studied on a variety of transition metal surfaces by various techniques by several authors (Blyholder 1964; Tracy 1972; Christmann *et al* 1974; Conrad *et al* 1974; Brundle 1975; Kishi and Roberts 1975; Ertl *et al* 1977; Moyes and Roberts 1977; Bradshaw 1979). CO is found to adsorb dissociatively on the early transition metals (to the left of the periodic table) and molecularly on the late transition metals (to the right of the periodic table). Based on this observation Broden *et al* (1976) suggested a boundary line in the periodic table which separates metals exhibiting dissociative chemisorption from those exhibiting molecular chemisorption. Benziger (1980) has attempted to rationalise this behaviour through a study of the heats of dissociative chemisorption. Dissociative chemisorption leads to the build-up of surface carbide and oxide (Benziger *et al* 1978), while molecular chemisorption has several interesting possibilities.

The HOMO of CO is a non-bonding orbital (5σ orbital) largely localised on the C atom. Immediately below it are the 1π and the 4σ orbitals that are responsible for bonding; the LUMO is the $2\pi^*$ orbital. According to the Blyholder (1964) scheme metal–CO bonding occurs through a synergetic bonding mechanism involving the $5\sigma \rightarrow$ metal and the metal $\rightarrow 2\pi^*$ charge transfer. Such a bonding scheme necessarily brings the 5σ level of the adsorbed CO closer to the 1π and 4σ levels which participate very little in the metal–CO bonding. Consequently, the ultraviolet photoelectron spectra of CO adsorbed on metals exhibit only two features (figure 5). The first of these features appearing at $\sim$ 7 eV has been assigned to the overlapping 5σ and 1π bands and the second feature appearing at higher energies to the 4σ band (Williams *et al* 1976). This assignment is now generally accepted.

Molecular adsorption of CO can occur on a variety of adsorption sites. While it is difficult to distinguish these in ultraviolet photoelectron spectra, studies of vibrational spectra by employing electron energy loss spectroscopy readily reveal the effect of the adsorption site. In figure 6 we show typical electron energy loss spectra of CO adsorbed on polycrystalline Cu, Pt and Pd. While Cu exhibits a single C–O stretching frequency close to 260 meV, Pt shows two bands at 260 and 248 meV (1 meV = 8·065 cm^{-1}). Pd shows only the 245 meV band, while Ni shows the 248 meV band at higher exposures. Based on the assignments of Sheppard and Nguyen (1978), we can readily assign the 260 meV stretching band to the terminally adsorbed CO molecule and the 248 meV band to the two-fold bridge bonded CO molecule. It is interesting that while Pt shows the coexistence of different CO adsorption sites, Ni exhibits a surface phase transition beyond a critical coverage value of $\theta > 0{\cdot}5$ (Andersson 1977).

In figure 7, we show another series of EEL spectra illustrating the variation in the metal reactivity to CO adsorption. While Mn exhibits dissociative chemisorption even at low temperatures (LT), Fe dissociates CO at room temperature and adsorbs it molecularly at lower temperatures (< 100 K). Co and Ni exhibit molecular adsorption

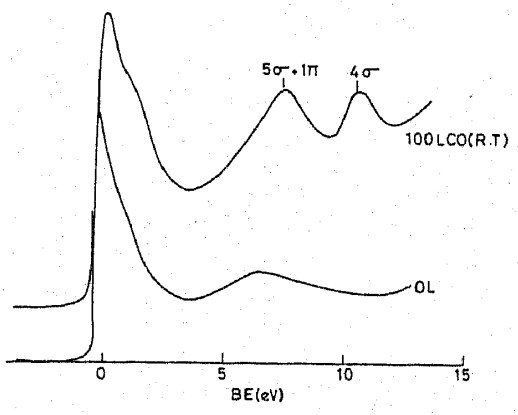

Figure 5. HeII photoelectron spectrum of adsorbed CO on a polycrystalline Ni surface.

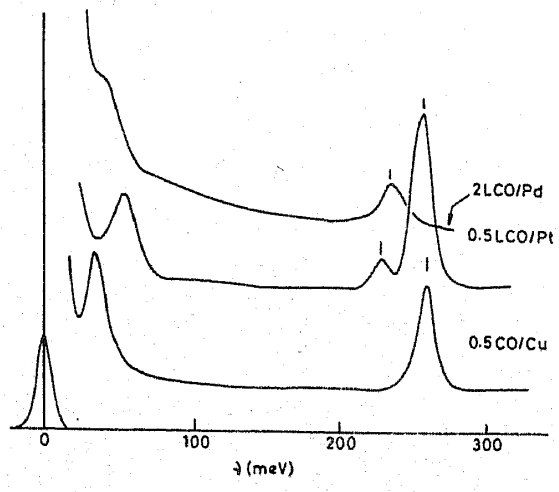

Figure 6. Vibrational EEL spectrum of CO adsorbed on polycrystalline sheets of Cu, Pt and Pd. The higher energy peaks correspond to terminally adsorbed CO while the low energy peak is due to the bridged CO.

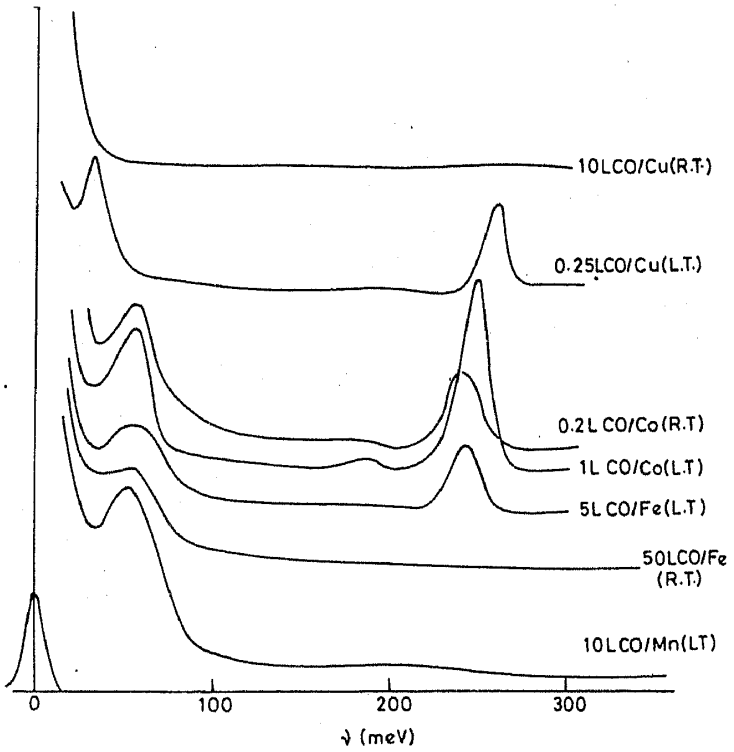

Figure 7. Vibrational electron energy loss spectra of CO adsorbed on polycrystalline sheets of first row transition metals.

at all temperatures upto 400 K, while Cu exhibits molecular adsorption only at low temperatures. Around room temperature (RT), Cu does not exhibit any ad-layer build-up. The reactivity of metals (with respect to dissociation of CO) therefore appears to vary in the order,

$$\text{Mn} \approx \text{Fe(RT)} > \text{Fe(LT)} > \text{Co} \approx \text{Ni} \approx \text{Cu(LT)} > \text{Cu(RT)}.$$

At one end, we have dissociative chemisorption and at the other no chemisorption. These results observed by us on polycrystalline metal foils are quite consistent with the single crystal data reported in the literature for Cu(100), Ni(100), Ni(111), Pd(100), Pt(111) and reviewed by Rao *et al* (1981a). It is generally found that the metal–carbon stretching frequency (appearing around 50 meV or lower) increases as the C–O stretching frequency decreases. This is what one would expect. The heat of adsorption as well as the 5σ level of CO vary systematically with the C–O stretching frequency (Rao *et al* 1981a).

Using higher energy electron beams it is possible to observe electronic excitations in adsorbed CO. While the energy of the intramolecular transition (5σ, $1\pi \rightarrow 2\pi^*$) of the adsorbed CO changes little on adsorption, the metal $E_f \rightarrow 2\pi^*$ (CO) excitation varies widely from metal to metal, increasing with increase in the ΔH_{ads}. This suggests that an increase in the strength of the metal–carbon bond causes an increase in the transition energy. These results have been discussed by Rao *et al* (1981b).

X-ray photoelectron spectra in the C(1*s*) and O(1*s*) regions are also useful to investigate CO adsorption on metal surfaces. While dissociative chemisorption gives rise to C(1*s*) and O(1*s*) spectra similar to those of carbides and oxides, the

corresponding features due to molecularly chemisorbed CO show a large variation from one metal to another. These variations have been related to heats of adsorption by Joyner and Roberts (1974).

C(1*s*) and O(1*s*) levels of CO show extensive satellite structure (Norton *et al* 1978). These satellites have been attributed to metal adsorbate charge-transfer excitations. These assignments are supported by the fact that no satellite is observed in the spectrum of the free CO molecule in this energy range. We have studied these satellites appearing next to the O(1*s*) level as a function of CO exposure on Cu, in order to understand their nature and origin more clearly.

We show in figure 8a, spectra in the O(1*s*) region of CO adsorbed molecularly on Cu. We clearly see three features A, B and C in the spectra. These features could be delineated by decomposition of the O(1*s*) peaks into gaussians using an error minimisation procedure; this procedure enables us to estimate the intensity of each feature as a percentage of the total intensity. We have plotted these intensities against the logarithm of exposure in figure 8b. At low exposures, peak A is of low intensity while peak B is intense and broad. With increase in CO exposure, peak A gains in intensity till it becomes the predominantly feature (beyond 100L), while peak B falls in

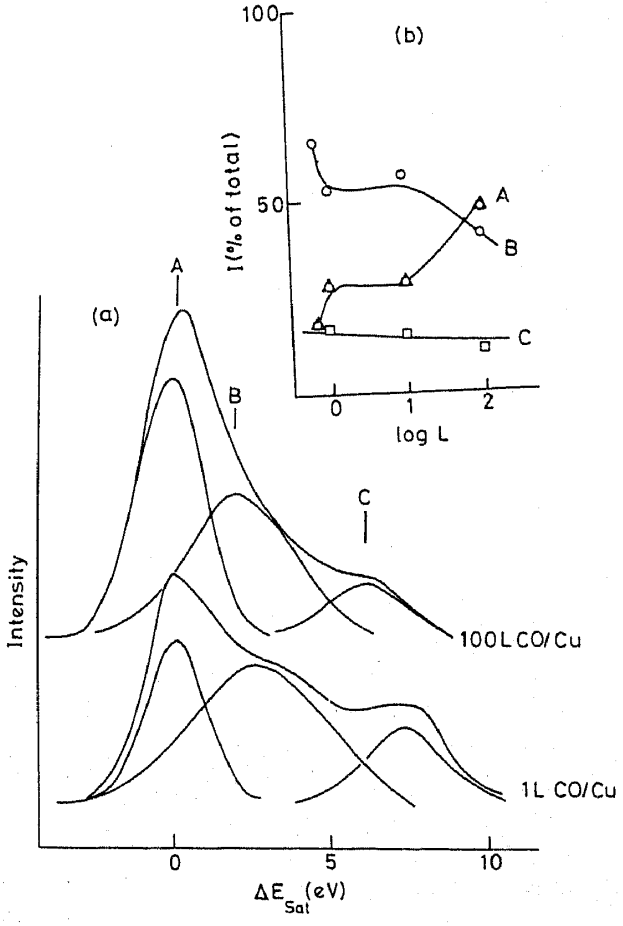

Figure 8. (**a**) O(1*s*) region of CO adsorbed on copper showing two types of satellites (B and C); A is the main O(1*s*) line. (**b**) Plots of relative intensities of A, B and C against logarithm of exposure.

intensity and gets substantially narrow. The intensity of C remains more or less constant. We assign these features based on the following considerations.

Satellites due to the adsorbate species can arise from metal-adsorbate as well as intra-adsorbate processes. At low exposures (sub-monolayer coverages) every adsorbate molecule is chemically bound to the metal surface. This causes metal-adsorbate charge transfer processes to dominate the satellite structure. At higher exposures, leading to multilayer coverage, adsorbate molecules not in the direct chemical environment of the metal out number those in the first monolayer, and these would contribute only to intra-adsorbate charge transfer interactions. The intensity of the satellite arising from metal-adsorbate charge transfer is therefore expected to decrease with increasing CO exposure, while the intensity of the satellite arising from intra-adsorbate charge transfer changes negligibly. Based on this premise, we assign peak B to a metal–CO charge transfer satellite while assigning peak C to a charge transfer process, predominantly involving adsorbed CO levels. Feature A, which becomes stronger with increasing exposure can be readily assigned to the main O(1*s*) line.

The width of feature B shows certain interesting changes with increasing exposure. With increase in exposure, feature B becomes progressively narrow (being 6 eV at 0·5 L and 4 eV at 100 L), while the widths of A and C remain almost unchanged. The broad feature at low exposure could arise from two or more peaks of comparable intensity corresponding to the presence of more than one species. On increasing the exposure, however, one of the peaks grows relatively faster than the other due to the preferential population of one of the species.

CO in sub-monolayer coverages forms clusters. At low coverages, the clusters are small and therefore the number of peripheral CO molecules is comparable to the number of CO molecules within the cluster. On increasing the coverage, the clusters grow and thereby the number of molecules inside the cluster increases relative to the number of peripheral CO molecules.

Apart from dissociation and molecular adsorption, disproportionation (Boudouard's reaction) has also been observed on a number of first row transition metals. This has been observed by UPS and XPS (Jagannathan *et al* 1980) and by Auger electron spectroscopy (Kamath *et al* 1982a). The reaction which can be written as $2CO \rightarrow C + CO_2$, leads to the formation of a surface carbide.

4. Results of MO calculations on CO adsorbed on transition metals

We have performed extended Hückel calculations for the adsorption of CO on 9-atom clusters of Fe, Ni, Pd and Cu. No geometry optimisation was attempted and the clusters were fixed at the experimental geometries obtained from LEED studies: Pd, (Behm *et al* 1979); Ni (Andersson and Pendry 1978a); Cu (Andersson and Pendry 1979b). For Fe, the geometries were obtained from the corresponding iron carbonyl complexes (Plummer *et al* 1978).

MO energies of free and adsorbed CO on various metals are shown in table 2. We find that the non-bonding 5σ level undergoes substantial stabilization on bonding to the metal clusters as found experimentally. At the same time, the 4σ and 1π orbitals remain relatively unchanged.

The chemisorption shift of the 5σ level is largest in the case of Fe and decreases progressively as we proceed to the right of the periodic table to Ni and Cu. This is

Table 2. Molecular orbital energies for CO in the free and adsorbed state for the M_9 cluster.

	Free Co	Fe	Ni	Pd*	Cu
3σ	−34·084	−34·248	−34·278	−34·539	−34·216
4σ	−18·609	−18·725	−18·750	−18·896	−18·746
1π	−16·384	−16·353	−16·357	−16·401	−16·355
				−16·386	
5σ	−13·221	−14·301	−14·223	−14·359	−14·196
$\Delta E^a_{5\sigma}$	—	1·08	1·0	1·138	0·975

* Calculation was carried out for the B_2 bridged site.
[a] ΔE denotes chemisorption shift.

Table 3. Molecular orbital energies of CO adsorbed on Fe_9 in different geometries.

	Terminal (T)	Bridged B_2	Bridged B_4
3σ	−34·247	−34·188	−34·145
4σ	−18·725	−18·669	−18·659
1π	−16·353	−16·387	−16·386
5σ	−14·301	−14·102	−13·997
2π	−9·385	−8·743	−8·592
$\Delta E^a_{5\sigma}$	1·08	0·881	0·776

[a] ΔE denotes chemisorption shift.

indicative of the higher reactivity of the Fe surface compared to the Ni and Cu and conforms to the experimental observations.

The MO diagram shows interesting changes as we change the geometry of the adsorption site. As we go from the terminal to the bridged geometry, the chemisorption shift of the 5σ level decreases significantly (table 3).

A variety of theoretical investigations of the adsorption of CO on various metals such as Cu, Pt, W and Ni have been reported in the literature. Calculations within the *ab initio* scheme (Janet and Goddard 1981) yield reliable values of Ni–C and C–O distances, as well as the heats of adsorption. Adsorption of CO on flat, stepped and kinked Ni surfaces has been investigated by Kobayashi *et al* (1981).

We have attempted to predict the nature of the possible metal-adsorbate charge-transfer satellites, based on our calculations. To simulate a cluster with a core hole, orbital energies belonging to the atomic centre where the core hole was created (O, in the present case) were depressed by about 3 eV. This appears reasonable as the orbitals localised on the atomic centre where the core hole is created, respond to the greatest extent to the positive potential of the core hole. The other orbitals are sufficiently screened and therefore do not change significantly.

The transitions were identified in conformity with the monopole selection rules. From such an examination, we are able to identify two transitions. The $2\pi^*$ level of CO (which is empty) interacts with the metal cluster orbitals to give rise to several bonding-antibonding pairs. The lower lying orbital in each pair (corresponding to ψ metal

$+\psi_{2\pi^*}$) is bonding with respect to the metal–CO bond and the higher energy level (corresponding to $\psi_{\text{metal}} - \psi_{2\pi^*}$) is antibonding with respect to the metal–CO bond. The $2\pi^*$ level of CO becomes partially filled in the metal–CO cluster owing to the transfer of the metal electrons into the $2\pi^*$ level. A predominantly metal $(d) \rightarrow 2\pi^*$ (CO) level charge transfer is possible within the framework of the monopole selection rules on the creation of a core hole at the O site. We find that such a transition occurs at an energy of 2·17 eV and corresponds to the feature B observed experimentally (figure 8a). We can also identify another pair of predominantly CO levels of π symmetry. Charge transfer arising from this pair of levels would be largely intra-adsorbate in nature and would appear at an energy separation of 5·6 eV. This compares with the feature C of the experimental spectrum.

5. Experimental results on the adsorption of oxygen on transition metals

Adsorption of oxygen on transition metals has been extensively studied in the last decade (see Wandelt 1982 and references therein). Adsorption of oxygen on transition metal surfaces yields a variety of species ranging from the oxide (O^{2-}) to molecular oxygen O_2. These species can be distinguished clearly from a study of UV and x-ray photoelectron spectra.

Dissociation of oxygen on metal surfaces is a commonly observed phenomenon. Dissociated oxygen can exist in the form of weakly chemisorbed triplet atomic oxygen, strongly chemisorbed singlet atomic oxygen or as the oxide (Spitzer and Luth 1982). Molecularly chemisorbed oxygen was unknown until 1980; the molecular species has been observed on Pt, Ag and other metal surfaces (Gland *et al* 1980; Backx *et al* 1981; Rao *et al* 1982; Spitzer and Luth 1982; Kamath and Rao 1984). Molecularly adsorbed oxygen may occur in the physisorbed state as well. Physisorbed molecular oxygen has been observed on Pd and Ni at 80 K by Kamath and Rao (1984). Physical adsorption of O_2 on surfaces of W, Ga etc at 20 K has also been reported (Schmeisser and Jacobi 1981).

The various oxygen species exhibit distinctly different features in their UV photoelectron spectra (figure 9). Molecular oxygen in the chemisorbed state shows three bands which can be assigned to the π_g^*, π_u and $2p\sigma_g$ levels (Rao *et al* 1982). Since the bands of the chemisorbed species due to π_u and $2p\sigma_g$ do not split as in the case of physisorbed O_2 on Ga (Schmeisser and Jacobi 1981), this dioxygen species can be assigned to the singlet oxygen. Physisorbed O_2, on the other hand, shows a more complex five peak structure, due to the splitting of features due to the π_u and $2p\sigma_g$ levels. This splitting arises because photoionisation from these orbitals in triplet O_2 leads to two final states which differ in their spin.

The molecular oxygen species is stable only at low temperatures and on warming dissociates to give triplet atomic oxygen. The triplet atomic oxygen causes a splitting of the peak due to the $2p$ level. At higher temperatures (close to room temperature), we observe a single band in the UV photoelectron spectrum due to strongly chemisorbed singlet atomic oxygen. These species can be identified in the x-ray photoelectron spectra as well. XPS binding energies of the various oxygen species are: oxide, 529 eV; chemisorbed atomic oxygen, 530·5 eV; chemisorbed molecular oxygen, 533·0 eV; physisorbed molecular oxygen, > 533 eV.

Electron energy loss spectra obtained from surfaces covered with oxygen provide

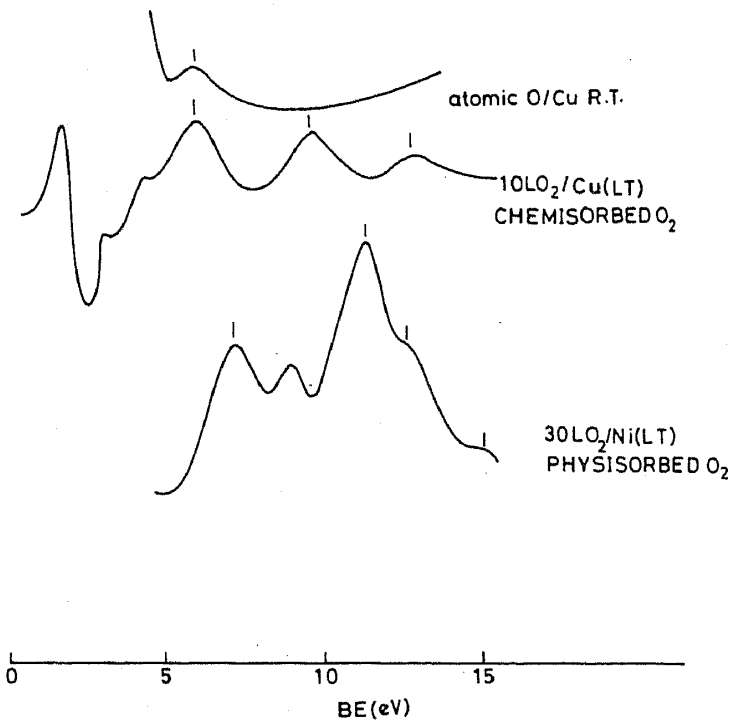

Figure 9. HeII photoelectron spectra of the various oxygen species adsorbed on metals.

interesting information. Dissociated oxygen exhibits the low energy metal-oxygen stretching mode while molecular oxygen shows bands due to the O–O stretching mode in addition to the M–O stretching band. The O–O stretch of adsorbed oxygen is greatly shifted from that of the free O_2 molecule, and occurs in the range of 78 meV (1 meV = 8·065 cm^{-1}) in the case of silver to 105 meV in the case of platinum. These stretching frequencies are indicative of a bond order less than unity (Kamath *et al* 1982b). On Pt, in addition to the 105 meV peak, another stretching frequency close to 80 meV is seen. This new species is considered to be the precursor to the dissociation of molecular oxygen (Avery 1983).

There has been much interest of late in the adsorption of oxygen on alkali metal modified transition metal surfaces. Several interesting oxygen species have been characterised on such metal surfaces (Goddard and Lambert 1981; Ayyoob and Hegde 1983) at conditions quite different from those required to stabilize them on unmodified transition metal surfaces.

Unlike alkali metals which enhance the adsorption of oxygen on Ag, by enhancing the sticking coefficient (Marbrow and Lambert 1976), absorbed S, Cl and atomic oxygen passivate transition metal surfaces (Koe and Madix 1982; Johnson and Madix 1981). The exact mechanisms of surface modification are not very well understood. While surface alkali atoms are thought to enhance the adsorption of dissociated oxygen, subsurface alkali metal incorporation is thought to stabilize the molecular dioxygen species (Kitson and Lambert 1981). The study of the adsorption of oxygen on clean and modified transition metal surfaces is therefore an important as well as an interesting problem.

6. Results of MO calculations on O_2 adsorbed on transition metal surfaces

Oxygen molecule is known to dissociate completely into atomic oxygen on a variety of metals (Rao *et al* 1980). Recent EELS results suggest the existence of a molecular precursor state which leads to dissociation of oxygen molecules on the metal surfaces (Avery 1983). We therefore sought to understand the mechanism of oxygen dissociation on metal surfaces. Interaction of oxygen with a metal cluster can occur at a variety of adsorption sites, most typical of these being the on-top and the hollow bridging sites. We have performed calculations on the interaction of oxygen at both these sites in linear as well as parallel geometries. The corresponding potential energy curves for Cu and Ag are shown in figures 10 and 11 respectively. On both the metals, the parallel on-top adsorption is preferred. Such a geometry would allow for a greater oxygen π^* orbital overlap with the metal orbitals, thus facilitating the metal $\rightarrow O_2$ (π^*) charge transfer.

Energy level diagrams for M_9O_2 clusters are shown for various geometries of adsorption in figure 12. There is a set of low lying orbitals mainly localized on the adsorbate. The *d* band as well as most of the orbitals remain unperturbed on bonding. Among those that undergo substantial changes on bonding are the dioxygen $2p\sigma$ orbital and the lowest orbital of the *s*–*p* band. The orbitals just above the *d* band also show considerable changes; these orbitals are of importance in accounting for adsorbate–adsorbant bonding.

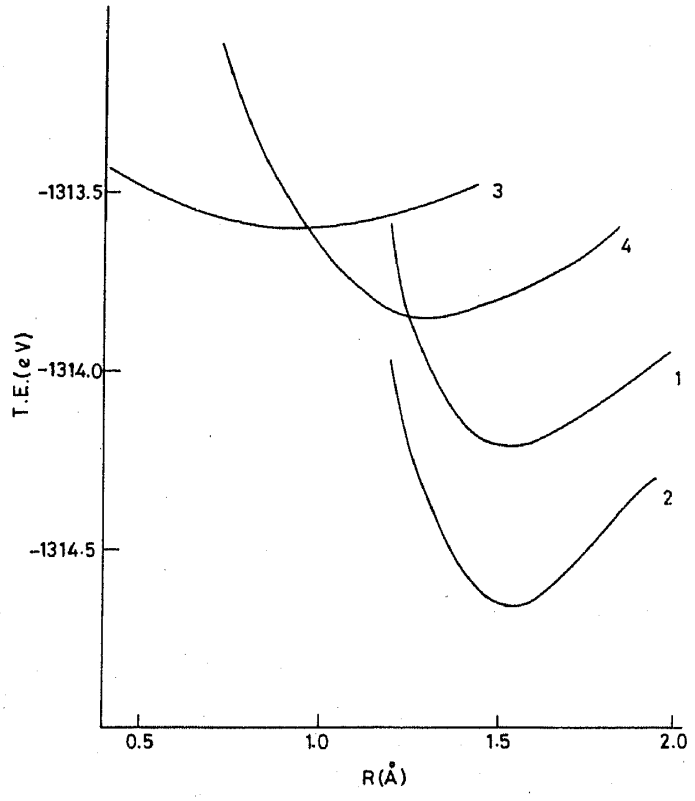

Figure 10. Potential energy curves for the interaction of molecular oxygen with a Cu_9 cluster in different geometries: (1) On-top linear, (2) On-top parallel; (3) 4-fold site linear; (4) 4-fold site parallel.

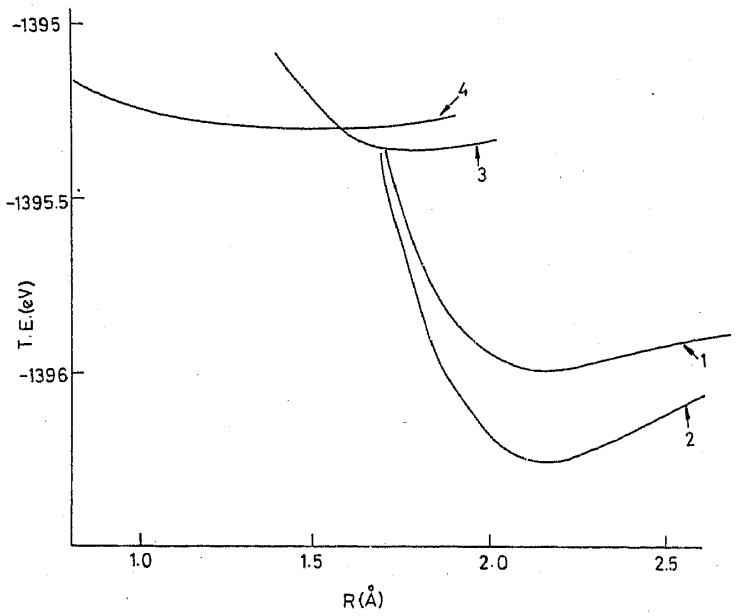

Figure 11. Potential energy curves for the interaction of molecular oxygen with a Ag_9 cluster. The geometries are the same as in figure 10.

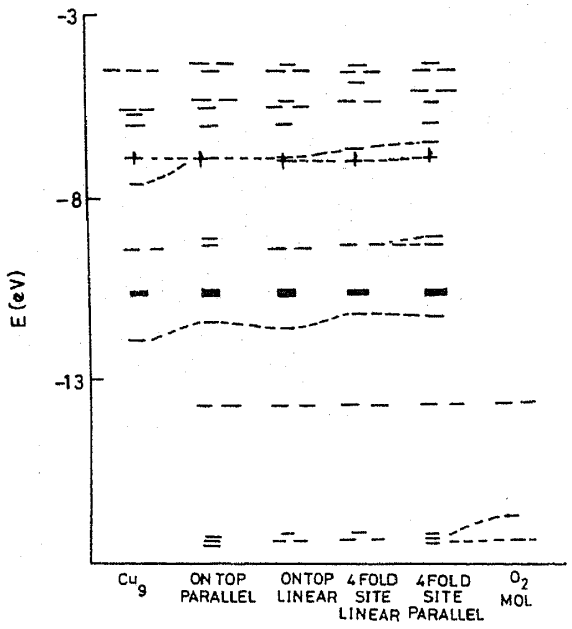

Figure 12. Molecular orbital diagrams for adsorbed molecular oxygen in various geometries on a Cu_9 cluster.

The molecular orbital diagrams show two salient features (in all the geometries): (a) A complete transfer of two electrons from the metal to the dioxygen π^* orbital and (b) stabilization of the oxygen $2p\sigma$ orbital. This clearly suggests that the dioxygen bond is greatly perturbed on adsorption on a metal surface. The π^* orbitals get fully filled causing a lowering of the bond order of dioxygen to unity. Stabilization of the $2p\sigma$

orbital also suggests a synergetic transfer of electron charge density from the $O_2(2p\sigma)$ level back to the metal orbitals. This would further reduce the O–O bond order to well below unity. Such a large lowering in the bond order has indeed been observed experimentally. HREELS studies of oxygen chemisorption on Pt and Ag show O–O stretching frequencies of 690 cm^{-1} (Avery 1983) and 640 cm^{-1} (Backx *et al* 1981) respectively which correspond to a bond order of around 0·8 (Kamath *et al* 1982b). Such a dioxygen species would be of a singlet variety (Spitzer and Luth 1982), similar to the dioxygen species observed in inorganic complexes (Vaska 1976). The dioxygen species in such complexes has been characterised to be of peroxo (O_2^{2-}) type with an O–O distance of 1·4 Å and $\nu_{(O-O)}$ of 800 cm^{-1}.

Avery (1983) has suggested that the dioxygen species having a stretching frequency of 690 cm^{-1} is the precursor to dissociation. Our calculations show that the on-top parallel species spontaneously dissociates, as any extension of the O–O bond leads to significant stabilization of the total energy of the system (figure 13). There is little difference in the dissociation profiles for the various geometries on Cu as well as Ag surfaces. The changes that occur in the molecular orbital diagram during the dissociation of the dioxygen species are depicted in figure 14.

Understandably, on increasing r(O–O), both $2p\sigma$ and $2p\pi$ destabilize greatly, while the antibonding $2p\pi^*$ levels stabilize. In addition, the $2p\sigma^*$ antibonding level is greatly stabilized (by ~ 19 eV) accompanying a transfer of metal electrons. These changes are ultimately responsible for the ready dissociation of oxygen on metal surfaces.

7. Effect of coadsorbed potassium and oxygen atoms on oxygen adsorption

We have investigated the adsorption of K and O atoms on two different symmetrically inequivalent sites of the Cu_9 cluster (the central metal atom and the edge atom of the

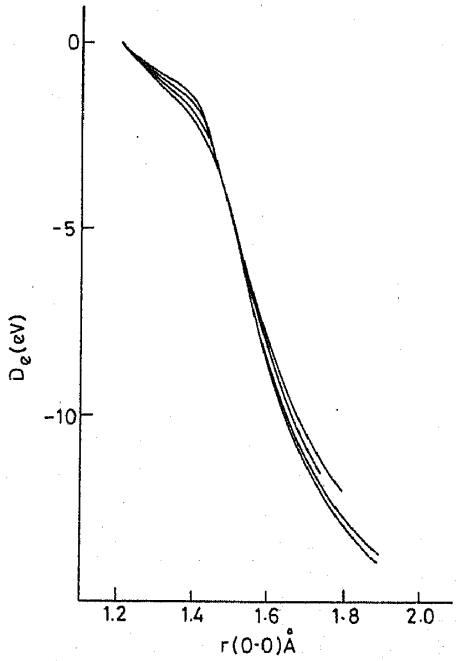

Figure 13. Dissociation profiles of the oxygen molecule in various geometries on a Cu_9 cluster (r(O–O) is the dioxygen bond length).

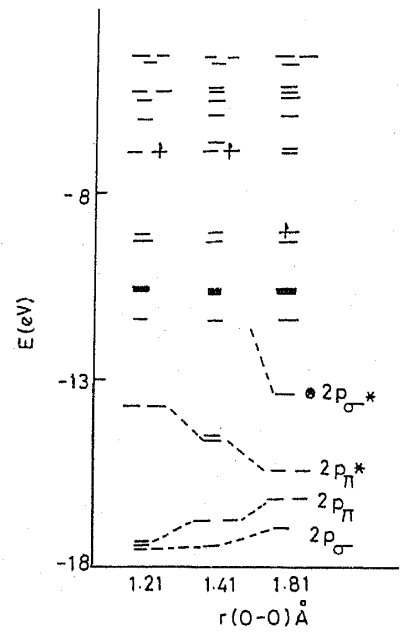

Figure 14. Changes in the MO diagram on lengthening of the dioxygen bond. The starred level is the $2p\sigma^*$ level of the dioxygen which stabilizes greatly.

upper plane). The charges on the atoms of the M_9X cluster, where X = K, O are tabulated in table 4. By a comparison of the values in table 4, with those in table 1, we see that on adsorbing a potassium or an oxygen atom, there is a substantial redistribution of the electron charge density inside the M_9 cluster. Adsorption of the alkali metal causes the Cu atoms of the cluster to acquire a negative charge due to electron donation from the potassium orbitals to the Cu orbitals. On adsorption of atomic oxygen, on the other hand, electron density is withdrawn from the M_9 cluster, resulting in the development of a positive charge on all the Cu atoms.

We have studied the on-top parallel geometry of adsorption of an oxygen molecule on the central Cu atom, when the coadsorbed potassium or oxygen atom is bonded to atom 4. Potential energy curves for the interaction of oxygen with modified Cu surfaces are shown in figure 15. In the presence of a coadsorbed K atom, the potential energy curve for the interaction of the oxygen molecule with the cluster is more shallow than that for the interaction with the unmodified surface. On the other hand, in the presence

Table 4. Average charges on the atoms within an M_9 X cluster. (X is bonded to an edge atom).

	Atom	Charge
X = Oxygen	O	−1·964
	Cu (1–5)	0·272
	Cu (6–9)	0·151
X = Potassium	K	0·992
	Cu (1)	0·022
	Cu (2–5)	−0·110
	Cu (6–9)	−0·144

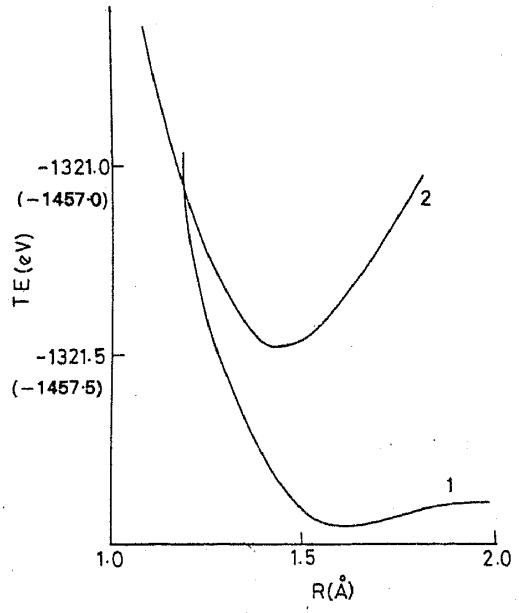

Figure 15. Potential energy curves for the interaction of molecular oxygen with a Cu_9 cluster modified by coadsorbed K atom (curve 1) and coadsorbed atomic oxygen (curve 2). The *Y* axis for curve 2 is marked in paranthesis. Geometry of interaction is on-top parallel.

of coadsorbed atomic oxygen, the potential energy curve is deep, showing stronger metal-dioxygen bonding. This is borne out by the dissociation profiles of molecular oxygen on the modified Cu surface shown in figure 16a. The dissociation energy of oxygen is enhanced by as much as 2 eV in the presence of coadsorbed K atoms and the reverse is the case in the presence of coadsorbed oxygen atoms. In figure 16b, we illustrate these differences graphically.

Enhanced adsorption of atomic oxygen has been observed on Ag surfaces in the presence of coadsorbed Na, K and Rb by thermal desorption spectroscopy (Goddard and Lambert 1981 and the references therein) and photoelectron spectroscopy (Ayyoob and Hegde 1983). The mechanism of oxygen dissociation on alkali metal modified transition metal surfaces would be similar to that on the unmodified metal surfaces. The alkali metal transfers an electron into the metal orbitals and this excess charge is available for transfer into the dioxygen antibonding levels, thus causing facile dissociation. The opposite would be the case in the presence of coadsorbed atomic oxygen.

On a modified surface, oxygen adsorption can occur on the promotor or the poison site. An examination of the charge on the atoms of the cluster shows that a K atom carries a positive charge on account of electron donation to the neighbouring Cu sites.

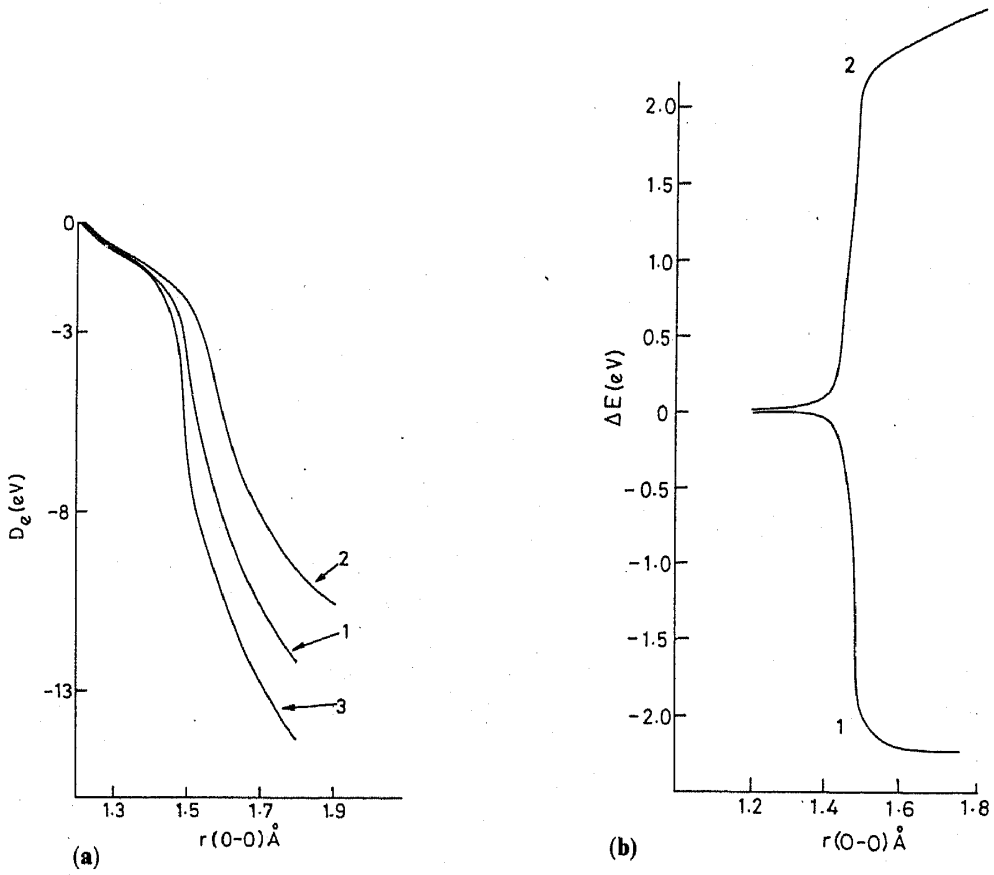

Figure 16. (**a**) Dissociation profiles of molecular oxygen in the on-top parallel geometry on a clean Cu surface (curve 1); in the presence of coadsorbed atomic oxygen (curve 2); in the presence of coadsorbed K (curve 3). (**b**) Graphical representation of the ease of dissociation and barrier to dissociation on modified Cu surface: In the presence of K (curve 1); in the presence of atomic O (curve 2).

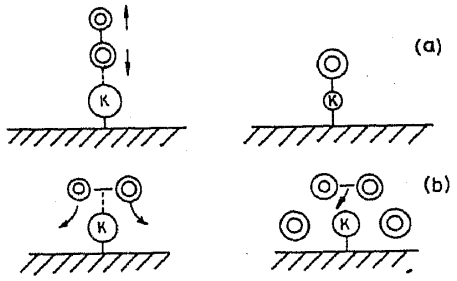

Figure 17. (**a**) Schematic representation of molecular oxygen adsorption with an on-top linear geometry on the K site and result of subsequent dissociation. (**b**) Schematic presentation of oxygen adsorption in the on-top parallel geometry on the K site and result of the subsequent dissociation.

Thus, K^+ would be a favourable site for oxygen adsorption. Oxygen can get adsorbed on the K site in the linear or the parallel geometry. Adsorption in the linear geometry on the K site followed by dissociation would lead to the formation of a potassium oxide layer causing the passivation of the surface (figure 17a). On the other hand, a parallel adsorption on the K site (figure 17b) followed by dissociation would lead to the migration of atomic oxygen to the Cu sites. This would leave the active K site open for further oxygen adsorption. This mechanism accounts for the increased sticking coefficient of oxygen on alkali metal modified surfaces. Potential energy curves for these two modes of oxygen interaction with the potassium site are shown in figure 18. It is clear that parallel adsorption is more favoured.

The mechanism of enhanced adsorption of atomic oxygen on alkali metal modified Ag surfaces is as follows. On account of its positive charge, the alkali metal provides the required attractive potential for the parallel adsorption of an oxygen molecule. The neighbouring Ag sites then donate electrons to oxygen antibonding levels causing the dissociation of the dioxygen species. Interaction of the oxygen molecule on the atomic oxygen poison site does not lead to stability, indicating the absence of bonding.

8. Effect of sub-surface alkali metal ions on oxygen adsorption

It has been recently postulated by Kitson and Lambert (1981), on the basis of thermal desorption experiments, that subsurface alkali metal atoms are responsible for stabilizing molecular oxygen on alkali metal modified Ag surfaces. It has also been observed that while K and Rb stabilize the dioxygen species, Na does not (Marbrow and Lambert 1976). We have carried out calculations for oxygen adsorption on a Ag_9 cluster in the presence of a sub-surface potassium ion. The Ag lattice was slightly distorted to accommodate the K ion. The dissociation profiles of dioxygen (figure 19) show that the sub-surface K enhances oxygen dissociation. This seems to be in variance with the conclusion of Goddard and Lambert (1981).

We would like to propose an alternate mechanism. Goddard and Lambert (1981) do not preclude the migration of the oxide ion into the sub-surface together with the alkali metal ion. This is in fact seen in the thermal desorption experiments where for all exposures of oxygen, there is a significant signal due to the sub-surface oxide species. The signal due to molecular oxygen, however, increases only at high exposures of

oxygen. At such exposures, there is a significant amount of sub-surface oxide. Molecular oxygen adsorption can, therefore, be considered to be due to the surface oxide which is passive to oxygen dissociation.

Acknowledgement

The authors thank the Department of Science and Technology and the University Grants Commission for support of this research.

References

Andersson S 1977 *Solid State Commun.* **21** 75
Andersson S and Pendry J B 1978a *Surface Sci.* **71** 75
Andersson S and Pendry J B 1978b *Phys. Rev. Lett.* **43** 363
Avery N R 1983 *Chem. Phys. Lett.* **96** 371
Ayyoob M and Hegde M S 1983 *Surface Sci.* **133** 516
Backx C, DeGroot C P M and Biloen P 1981 *Surface Sci.* **104** 300
Baetzold R C 1971 *J. Chem. Phys.* **55** 4355
Behm R J, Christmann K, Ertl G, Van Hove M A, Thiel P A and Weinberg W H 1979 *Surface Sci.* **88** L59
Benziger J B, Koe E I and Madix R J 1978 *J. Catal.* **54** 414
Benziger J B 1980 *Appl. Surface Sci.* **6** 105
Blyholder G 1964 *J. Chem. Phys.* **68** 2772
Bradshaw A M 1979 *Surface Sci.* **80** 215
Broden G, Rhodin T N, Brucker C, Benbow R and Huyrich Z 1976 *Surface Sci.* **59** 593
Brundle C R 1975 *J. Electron Spectrosc. Rel. Phenom.* **7** 484
Christmann K, Schober O and Ertl G 1974 *J. Chem. Phys.* **60** 4719
Clementi E and Raimondi D L 1963 *J. Chem. Phys.* **38** 2686
Conrad H, Ertl G, Koch J and Latta E E 1974 *Surface Sci.* **43** 462
Ertl G, Neumann M and Streit K M 1977 *Surface Sci.* **64** 393
Gland J L, Sexton B A and Fisher G B 1980 *Surface Sci.* **95** 587
Goddard P J and Lambert R M 1981 *Surface Sci.* **107** 519
Hoffmann R 1963 *J. Chem. Phys.* **39** 1397
Jagannathan K, Srinivasan A, Hegde M S and Rao C N R 1980 *Surface Sci.* **99** 309
Janet N A and Goddard W A 1981 *Surface Sci.* **110** L615
Johnson S and Madix R J 1981 *Surface Sci.* **103** 361
Joyner R W and Roberts M W 1974 *Chem. Phys. Lett.* **29** 447
Kamath P V, Yashonath S, Srinivasan A and Rao C N R 1982a *Appl. Surface Sci.* **10** 559
Kamath P V, Yashonath S, Srinivasan A, Basu P K and Rao C N R 1982b *J. Indian Chem. Soc.* **59** 153
Kamath P V and Rao C N R 1984 *J. Phys. Chem.* **88** 464
Kishi K and Roberts M W 1975 *J. Chem. Soc. Faraday Trans.* I **71** 1715
Kitson M and Lambert R M 1981 *Surface Sci.* **109** 60
Kobayashi H, Yoshida A and Yamaguchi M 1981 *Surface Sci.* **107** 321
Koe E I and Madix R J 1982 *Surface Sci.* **112** 273
Marbrow R A and Lambert R M 1976 *Surface Sci.* **61** 329
Moyes R B and Roberts M W 1977 *J. Catal.* **49** 216
Norton P R, Tapping R L and Goodale F W 1978 *Surface Sci.* **72** 33
Plummer E W, Salaneck W R and Miller J S 1978 *Phys. Rev.* **B18** 1673
Rao C N R and Hegde M S 1981 in *Preparation and characterization of materials* (ed.) J M Honig and C N R Rao (London: Academic Press) p. 161
Rao C N R, Kamath P V and Yashonath S 1982 *Chem. Phys. Lett.* **88** 13
Rao C N R, Sarma D D and Hegde M S 1980 *Proc. R. Soc. (London)* **A370** 269
Rao C N R, Srinivasan A and Jaganathan K 1981a *Int. Rev. Phys. Chem.* **1** 45
Rao C N R, Srinivasan A and Jaganathan K 1981b *Indian J. Chem.* **A20** 72
Schmeisser D and Jacobi K 1981 *Surface Sci.* **108** 421

Sheppard N and Nguyen T T 1978 in *Advances in IR and Raman spectroscopy*, (ed.) R J H Clark and R E Hester (London: Heyden) Vol. 5, p. 67
Spitzer A and Luth H 1982 *Surface Sci.* **118** 121
Tracy J C 1972 *J. Chem. Phys.* **56** 2736
Vaska L 1976 *Acc. Chem. Res.* **9** 175
Wandelt K 1982 *Surface Sci. Rep.* **2** 1
Williams R M, Butcher P, Wood J and Jacobi K 1976 *Phys. Rev.* **B14** 3215
Zerner M and Goutermann M 1966 *Theor. Chim. Acta* **4** 44